Structure-conductivity relationship of PrBaMnMoO<inf>6-δ</inf> through in-situ measurements: A neutron diffraction study

Ceramics International 47 (2021) 541–546

Contents lists available at ScienceDirect

Ceramics International

journal homepage: www.elsevier.com/locate/ceramint

Structure-conductivity relationship of $PrBaMnMoO_{6-\delta}$ through *in-situ* measurements: A neutron diffraction study

Shammya Afroze[a,b], Nico Torino[b], Md Sumon Reza[a], Nikdalila Radenahmad[a], Quentin Cheok[a], Paul F. Henry[c,d], Abul K. Azad[a,*]

[a] Faculty of Integrated Technologies, Universiti Brunei Darussalam, Jalan Tungku Link, Gadong, BE 1410, Brunei Darussalam
[b] Department of Chemistry and Chemical Engineering, Chalmers University of Technology, SE-412 96, Gothenburg, Sweden
[c] ISIS Pulsed Neutron & Muon Facility, Rutherford Appleton Laboratory, Harwell Campus, OX11 0QX, United Kingdom
[d] Department of Chemistry – Ångström Laboratory, Inorganic Chemistry, Uppsala University, 751 21, Uppsala, Sweden

ARTICLE INFO

Keywords:
In-situ conductivity
Neutron diffraction
Double perovskite
$PrBaMnMoO_{6-\delta}$
SOFC electrode

ABSTRACT

The structural and electrochemical properties of the double perovskite-type oxide, $PrBaMnMoO_{6-\delta}$, was investigated using neutron diffraction with *in-situ* conductivity measurement under a dry Argon atmosphere from 25 °C to 700 °C. A Rietveld refinement of the neutron diffraction data confirmed monoclinic symmetry in the $P2_1/n$ space group. Rietveld refinement also confirms the unit cell parameters of a = 5.6567 (1) Å, b = 5.6065 (2) Å, c = 7.9344 (1) Å and β = 84.43° with reliable atomic positions and refinement factors (R-factors). Neutron diffraction data refinement shows two minor phases (< 5%), an orthorhombic AB_2O_5 type phase of $PrMn_2O_5$ in the *Pbam* (No. 32) space group with unit cell parameters, a = 7.9672 (1) Å, b = 8.9043 (2) Å and c = 5.8540 (1) Å and a scheelite phase of $BaMoO_4$ in the tetragonal $I4_1/a$ (88) space group with the unit cell parameters, a = b = 5.9522 (1) Å, and c = 12.3211 (2) Å. Morphological images revealed a porous and intertwined microstructure. In-situ conductivity measurement shows that the total conductivity of this material was 130.84 Scm^{-1} at 700 °C.

1. Introduction

The solid oxide fuel cell (SOFC) is considered one of the most viable energy conversion devices due to its high energy efficiency, fuel flexibility, and near-zero-emission operation [1,2]. SOFCs generate electricity through electrochemical reactions, directly from the oxidation of fuels [3,4]. It can use hydrogen, hydrocarbon [5], natural gas (methane), syngas [6,7], and biogas [8,9] as fuel and is not restricted by the Carnot cycle. It has also become a promising technology for a wide range of uses, especially in stationary situations; for example, they can be used to produce combined heat and power (CHP) for residential households [10,11] and in medium-scale distributed electricity generation [12]. The research in optimizing common materials for use in SOFCs is a vital topic in materials science in order to improve long-term stability, reduce costs, and also provide more material alternatives. A lot of emphasis is placed upon anode research because the performance of the SOFC is heavily-dependent upon it as the anode is where fuel is fed into the SOFC [13,14]. Conventionally, Ni-based composites are most commonly-used to construct SOFC anodes as these composites yield high activity for pure H_2 oxidation and they are also good current collectors [15]. An example of such would be Ni-substituted yttria-stabilized zirconia (YSZ) cermet. However, Ni-YSZ results in poor redox cycling constancy as Ni is deactivated in NiO by rapid oxidation [16] in addition to its sensitivity to sulfur poisoning [17,18]. As such, many types of materials have been investigated to find a suitable replacement material for SOFC anode construction. Generally, SOFC requires mingled electronic-ionic conducting oxides for both anode and cathode materials [19].

Many novel perovskite materials (ABO_3) have already been developed for the SOFC electrode [20–22] to overcome the problems of Ni-YSZ. One of the significant advantages of perovskite materials is high electrical conductivity. In this paper, the double perovskite material ($AA'BB'O_6$) [23,24] is the main focus due to its structural versatility, chemical-, physical-, and thermal stability during SOFC applications. B and B′ sites are occupied with different cations based on their valence and ionic radii [25].

Various rare-earth cations have been introduced at the A-site to obtain enhanced performance. Among them, the Pr-containing materials are suitable because of high stability and chemical compatibility with electrolytes [26–29]. A mixture of rare-earth and alkaline-earth A-

* Corresponding author.
E-mail address: abul.azad@ubd.edu.bn (A.K. Azad).

https://doi.org/10.1016/j.ceramint.2020.08.161
Received 5 May 2020; Received in revised form 17 August 2020; Accepted 17 August 2020
Available online 18 August 2020

sites enables mixed-valence states in double perovskites and this demonstrates higher electronic conductivity. As an example, Pr^{3+} and Ba^{2+} cations have alternating layers that make them ideal as electrode materials for SOFCs [30]. The oxygen atoms in the PrO_x plane create many oxygen-vacant sites in the crystalline structure which facilitates the ionic and electronic conductivity [31].

In this work, we have performed *in-situ* conductivity-structure measurements of $PrBaMnMoO_{6-\delta}$ to understand the changes of structure and conductivity with temperature. Structure determination was conducted by neutron powder diffraction (NPD) and conductivity was measured by Electrochemical Impedance Spectroscopy (EIS). Neutron powder diffraction (NPD) is a potent procedure that is used for its ability to detect light molecular weight elements [32] such as hydrogen and oxygen in order to analyze the structure of ion-conducting solids. Also, neutron diffraction can be used to detect the scattering from oxygen which is shown as additional peaks and consequently, the changes to the crystalline system. In the case of oxide materials, this scattering occurs due to oxygen anions deflecting the neutrons as they penetrate deep into the material structure [33]. For *in-situ* measurements, electronic-ionic conductivity was measured during neutron diffraction data collection at different temperatures. The time-of-flight (TOF) neutron data was collected and analyzed to obtain a complete diffraction pattern with a small scattering angle, which enabled the rapid collection of long-range data. Based on the structural analysis, the electrical properties of the crystal structure is essential for understanding the process of oxygen transport.

Materials development for SOFCs is an on-going process to get better performance. However, in-situ conductivity-diffraction measurement is a unique process to understand the under laying mechanism and very few works have been performed until now. The purpose of this work is to investigate the temperature-dependent changes on the crystalline structure as a result of changes in electronic-ionic conductivity and to form a correlation between the electrochemical and structural properties [34]. As far as we know, *no such study has been* piloted, in which the *in-situ* technique is applied to understand the process occurring in the SOFC on this double perovskite composition.

2. Methods

The double perovskite $PrBaMnMoO_{6-\delta}$ material was synthesized using a solid-state synthesis process [35–38]. Stoichiometric amounts of Pr_6O_{11} (≥99.99%, Aldrich), $SrCO_3$ (≥99.90%, Aldrich), MnO (≥99.50%, Aldrich), and MoO_3 (≥99.50%, Aldrich) were mixed in an agate mortar & pestle using ethanol as the mixing medium. The well-mixed powders were then pre-sintered in a furnace for 10 h at 650 °C. The powders were re-ground using the agate mortar & pestle, pressed into small discs and heated at 900 °C for 12 h. The pellets were re-fired at 1200 °C and finally, at 1400 °C for 12 h each. The sample was heated in 5% H_2 at 1000 °C for 5 h to check the stability of the sintered product at reducing atmosphere. The heating and cooling rate was 5 °C/min for all heating cycles and conducted under Argon atmosphere [2].

The phase structure was first determined using X-ray powder diffraction by a Bruker axs-D8 Advance diffractometer. The data was collected in the 2θ range from 10° to 79.995° with increments of 0.02° per second and was analyzed by Rietveld analysis using Fullprof software [39]. The background was demonstrated using the 6-coefficient polynomial function and the peak shape was deliberated as pseudo-Voigt.

The crystalline structure and conductivity of $PrBaMnMoO_{6-\delta}$ were studied using *in-situ* Neutron Diffraction and impedance spectroscopy cell at the ISIS Neutron and Muon Source at the STFC Rutherford Appleton Laboratory in Oxfordshire, UK using the POLARIS time-of-flight (TOF) diffractometer [40,41]. The sample was loaded into 8 mm diameter cylindrical vanadium can, which was bound in a quartz tube and sealed with a Cu gasket. The measurements were performed at different temperatures (ranging from 25 °C to 700 °C). The temperature was recorded using a thermocouple (similar setup was shown by Kinyanjui et al.) [42]. The sample was heated up to 700 °C by two resistive coils above and beneath the sample container. The experiment was carried out at 1 mbar pressure, controlled by an inlet and outlet valve in a vacuum. The TOF data was analyzed by Rietveld refinement with GSAS-II software [43] using the data collected at bank 2 (up to 7 Å). The background parameters, cell parameters, scale factor, profile parameters (type 3, as applied in GSAS), site occupancy factors (SOF), atomic displacement factors (ADP), atomic coordinates and phase fractions were refined to get complete structural information at different temperature.

The morphological structure was analyzed using scanning electron microscopy (SEM) to determine its porosity. A carbon layer was coated onto the sample to avoid overcharging as the sample was very conductive. The images (both surface and cross-sectional) of the pellet were taken with a JSM-7610F (Japan Electron Optics Laboratory Co. Ltd., Japan) [44]. The SEM images provided an excellent, high contrast view of the pellet.

In-situ conductivity was measured using a Solartron impedance analyzer coupled with a Frequency Response Analyzer (FRA) in the frequency range of 0.1 Hz–5 MHz at AC amplitude of 100 mV. The electrochemical impedance software Z-view was used to analyze the impedance data. The measurements were carried out in a dry Argon atmosphere (Ar gas was passed through paraffin). The impedance measurement jig, which was designed and built at ISIS [34], was mounted vertically in the furnace and placed into the sample tank. The temperature was set in regular intervals from 25 °C to 700 °C (25 °C, 100 °C, and 200 °C, up to 700 °C) and the sample remained at each temperature for 2 h to allow for thermal equilibrium. The neutron diffraction data and impedance spectra were then collected at the same time to determine whether there were any changes in structure and conductivity. Fig. 1 shows the picture and schematic diagram of the in-situ experimental setup.

3. Result and discussions

The double perovskite-type polycrystalline $PrBaMnMoO_{6-\delta}$ was prepared using solid-state reaction method using final sintering temperature of 1400 °C under Argon atmosphere. Then the sample was heated at 1000 °C in reducing atmosphere (5% H_2/Ar) for 5 h. The preliminary structural determination was carried out by X-ray powder diffraction (XPD). Indexing and cell refinement of the XRD data showed that the material crystallizes in two different phases namely, double perovskite ($PrBaMnMoO_{6-\delta}$) and scheelite ($BaMoO_4$). The Rietveld analysis of XPD data shows a monoclinic structure of $PrBaMnMoO_{6-\delta}$ in the space group $P2_1/n$ (no. 14) and a tetragonal structure of $BaMoO_4$ in the space group $I4_1/a$ (no. 88) [45]. However, neutron diffraction is more powerful tool to get accurate structural information for its high sensitivity for light atoms, scattering factor and non-absorbance in atomic electron cloud. Neutron diffraction is useful for studying compounds that contain heavy atoms that strongly absorb X-ray radiation.

The Rietveld refinement of the NPD data shows one additional orthorhombic phase of $PrMn_2O_5$ in the *Pbam* space group. The main phase was monoclinic $PrBaMnMoO_{6-\delta}$ in the $P2_1/n$ space group which comprises more than 95% of the material. So, the final structure from neutron diffraction show three distinct phases: (i) monoclinic structure for $PrBaMnMoO_{6-\delta}$, orthorhombic structure for $PrMn_2O_5$ and tetragonal structure for $BaMoO_4$. The lattice parameters of the main phase was as follows: a = 5.6567 (1) Å, b = 5.6065 (2) Å, c = 7.9344 (1) Å and β = 84.4300° (monoclinic, $P2_1/n$ space group). This cell parameters are related to the basic perovskite as $a \approx \sqrt{2}a_p$, $b \approx \sqrt{2}a_p$, $c \approx 2a_p$, $\beta \neq 90°$. Table 1 shows the atomic positions, isotropic thermal parameters and fractional occupancies of the primary phase. The refinement of the 2nd phase ($PrMn_2O_5$) shows that this phase crystalizes in the AB_2O_5 type structure which can be refined in the orthorhombic *Pbam* (No. 32) space group. The unit cell parameters were, a = 7.9672 (1) Å, b = 8.9043 (2)

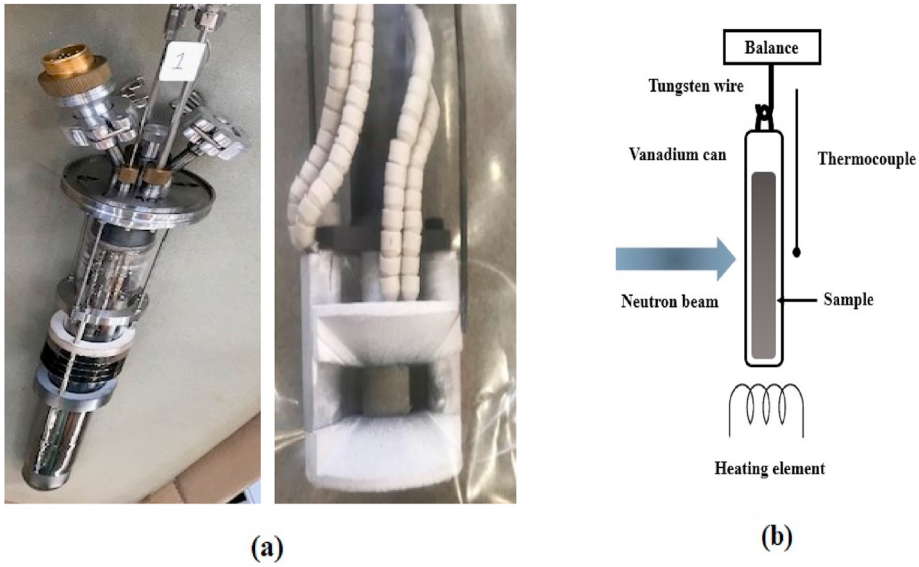

Fig. 1. (a) In-situ sample environment for $PrBaMnMoO_{6-\delta}$ in an inert atmosphere. (b) Schematic illustration of the in-situ experimental setup at ISIS.

Table 1
List of atomic positions, isotropic temperature factors, and fractional occupancies for the main phase $PrBaMnMoO_{6-\delta}$ (space group, $P2_1/n$) from neutron diffraction data at room temperature.

Atomic	x	y	z	Uiso	Fractional occupancy
Pr	0.9490 (2)	0.4729 (1)	0.1195 (2)	0.0057 (3)	1.000
Ba	0.9490 (2)	0.4729 (1)	0.1195 (2)	0.0350 (4)	1.000
Mn	0.5000	0.0000	0.5000	0.0051 (4)	1.000
Mo	0.5000	0.0000	0.0000	0.2474 (1)	1.000
O1	0.2789 (1)	0.6370 (1)	0.2115 (1)	0.0616 (1)	1.896 (3)
O2	0.7358 (2)	0.3304 (2)	0.0151 (1)	0.1076 (2)	2.273 (2)
O3	0.2250 (1)	0.0625 (1)	0.9460 (3)	0.0219 (2)	1.886 (2)

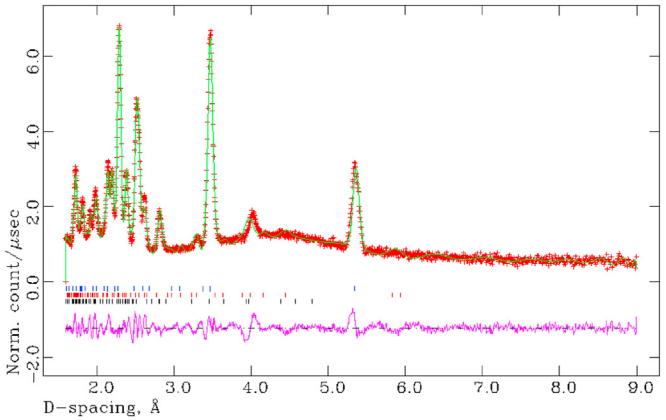

Fig. 2. Rietveld refinement profile of the neutron diffraction data collected at room temperature (295K) for $PrBaMnMoO_{6-\delta}$. Main phase: monoclinic, $P2_1/n$ space group, 2nd phase: orthorhombic, *Pbam* space group, 3rd phase: tetragonal, $I4_1/a$ space group. Observed data (red + sign), calculated profile (green line), Bragg positions (vertical lines) and difference pattern (purple line in the bottom) are shown. (For interpretation of the references to colour in this figure legend, the reader is referred to the Web version of this article.)

Å and c = 5.8540 (1) Å. The 3rd phase of $BaMoO_4$ was crystallized as a scheelite type structure in the $I4_1/a$ space group with the unit cell parameters, $a = b$ = 5.9522 (1) Å, and c = 12.3211 (2) Å. All three phases were refined simultaneously to get reliable structural parameters and refinement factors (R-factors) where all peaks were indexed with proper intensity matching, as shown in Fig. 2.

The preliminary refinement results demonstrated that Mn was situated at the 2a crystallographic site, while Mo originated from the 2c site. O2 displayed larger thermal displacees than O1 because of different oxygen sites. Fractional occupancies of cations were kept fixed due to small variations from their nominal occupancies. The Mn:Mo ratio was refined separately without applying any constraints which shows no mixing in their sites. Site occupancy factors (SOF), atomic displacement factors (ADP) were refined in different cycles due to their strong correlation. The oxygen vacancies are located in the praseodymium layers. A scheelite phase impurity is common in double perovskite type materials (e.g. $AA'MnMoO_6$) especially for the rare-earth-containing compounds as found in Ba_2MMoO_6 (M = Fe, Co, Mn, Ni) [46]. The unit cell volume depends on the Pr^{3+}:Ba^{2+} ratio which is strongly correlated to the Mn^{2+}:Mo^{6+} ratio [47]. Table 2 shows the cell parameters and refinement factors in elevated temperatures.

The presence of oxygen vacancies in the Pr layer was observed due to the mixed-valence state of Pr/Ba cations which also related to the mixed valence state of Mn and measure temperature. U_{iso} of all the atoms were refined isotropically. The refinement of oxygen occupancies for three sites improved the matching of the peak intensities. The Rietveld refinement of the neutron data collected at 200 °C, 400 °C and 700 °C (as shown in Fig. 3) confirmed that there were no structural phase changes at higher temperatures. However, there was a small increase in unit cell parameters. The variation of temperature has a significant effect on the physical properties of double perovskites, which is very important for fuel cell applications. At high temperature, the conductivity increases.

SEM imaging is a suitable method to categorize the microstructure

Table 2
Unit cell parameters, χ^2 values, and R-factors of $PrBaMnMoO_{6-\delta}$ at selected temperatures.

Parameters	RT	200	400	700
Space group	$P2_1/n$	$P2_1/n$	$P2_1/n$	$P2_1/n$
a (Å)	5.65679 (1)	5.76210 (2)	5.68380 (1)	5.6646 (0)
b (Å)	5.62133 (2)	5.56072 (1)	5.48287 (1)	5.6474 (2)
c (Å)	7.94766 (2)	7.95738 (1)	7.86343 (2)	7.9931 (3)
β (°)	84.43000	83.00640	84.50310	84.43610
χ^2	4.28500	3.58800	3.03000	2.24200
R_p%	7.22000	7.28000	7.63000	7.29000
R_{wp}%	8.03000	8.89000	8.34000	7.34000

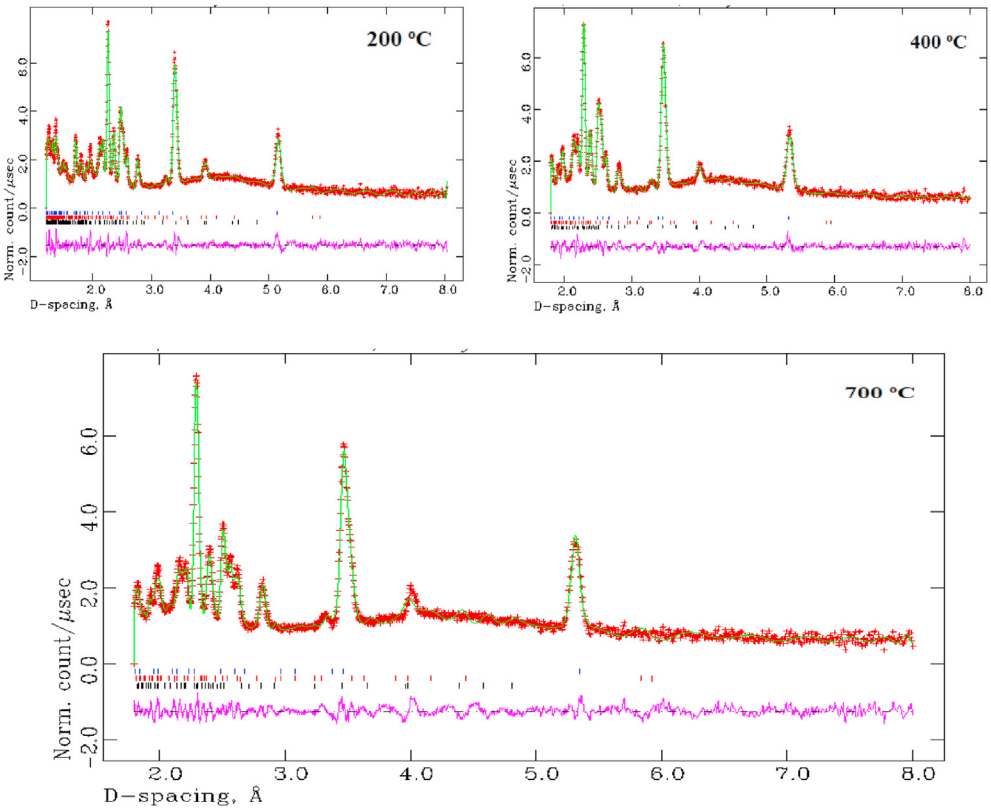

Fig. 3. Neutron diffraction refinement plots at 200 ˚C, 400 ˚C, and 700 ˚C, respectively for $PrBaMnMoO_{6-\delta}$. The main phase and impurity phases were same up to 700 ˚C. Measured data (red), a calculated pattern (green line), difference pattern (purple line), and Bragg positions (vertical lines) are observed in the model. (For interpretation of the references to colour in this figure legend, the reader is referred to the Web version of this article.)

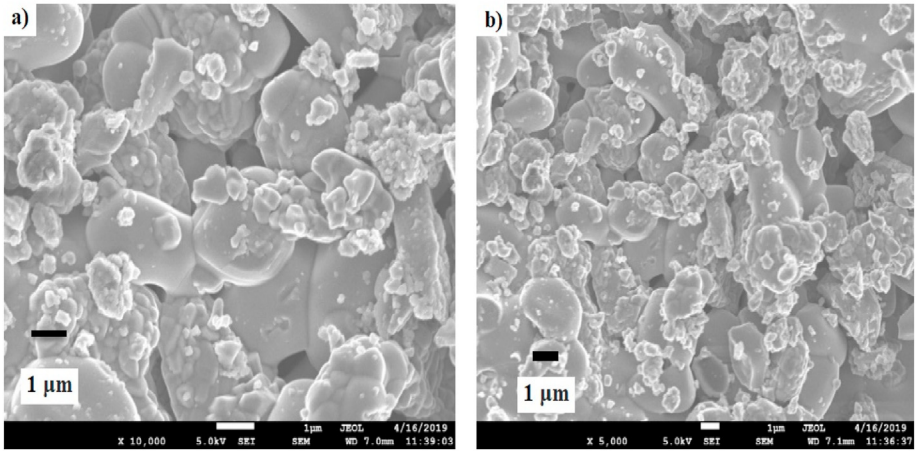

Fig. 4. SEM micrographs for $PrBaMnMoO_{6-\delta}$ pellet at a voltage, 5.0 kV, (a) SEM images of the pellet surface with a working distance (WD) 7.0 mm, scale bar 1 μm with magnification 10,000X (b) SEM images of the cross-sectional pellet with working distance (WD) 7.1 mm, scale bar 1 μm with magnification 5,000X.

of perovskite-type oxide materials [48]. The microstructure of the ceramic materials is greatly affected by A-site and B-site cations as well as by the synthesis and sample preparation procedure [49]. Fig. 4 illustrates the SEM image of the pellet surface (a) and cross-section of the pellet (b) at different magnifications. Both images show a porous morphology. The secondary phases are well-distributed throughout the material with the average grain size approximately 1 μm. This is significant as the grain boundary facilitates and expedites the conduction of fuel during the three-phase reaction in a fuel cell anode [50].

In-situ conductivity allows the change in the crystal structure and conductivity to be measured simultaneously. As a result, the change in lattice parameters, as well as unit cell volume due to thermal expansion [48] and electron-ion movement, can be quantified. It can be understood from the literature that the rare-earth perovskite oxide materials show satisfactory electrochemical performance. The presence of bulk, grain-boundary and electrode resistance in the prepared samples showed more than one semicircle appeared in electrochemical impedance measurements in a dry Argon atmosphere. The total conductivity can be measured using the following equation [51,52]:

$$\sigma = \frac{1}{\rho} = \frac{L}{RA} \tag{1}$$

where σ is the conductivity, ρ is the resistivity, L is the length, R is the resistance, and A is the cross-sectional area of the pellet.

It can be observed from electrochemical impedance spectroscopy that the conductivity of the sample increases with temperature (Fig. 5). The conductivity of $PrBaMnMoO_{6-\delta}$ was calculated (fitted) from the impedance spectra by Z-view software modelled with an equivalent circuit. The value of R_s is the Ohmic resistance, while R_1 is the bulk resistance [53] in the fitted equivalent circuit (Fig. 5 inserted). R_2 and

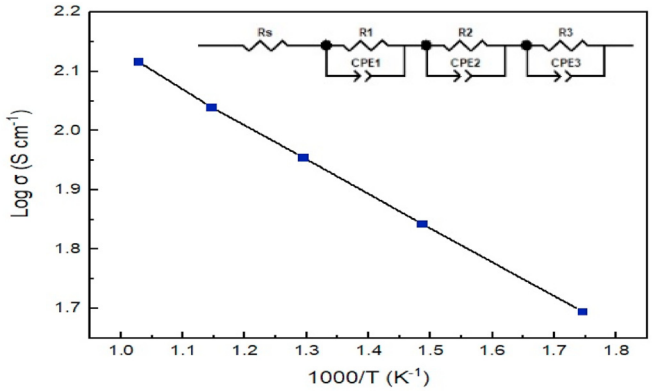

Fig. 5. Arrhenius plot of conductivity of $PrBaMnMoO_{6-\delta}$ at 25–700 °C under dry Ar.

R_3 are resistances from the grain boundary and the electrode, respectively. A detailed analysis of the impedance spectra has been reported [54,55]. The conductivity values can be extracted from the data. Fig. 5 exhibits the Arrhenius plot of the $PrBaMnMoO_{6-\delta}$, where the activation energy of the sample was 0.116 eV measured under dry Argon environment.

The obtained conductivity values of $PrBaMnMoO_{6-\delta}$ were 130.84, 109.69, 90.21, 69.71, and 49.59 Scm^{-1} at 700 °C, 600 °C, 500 °C, 400 °C, and 300 °C, respectively. We observed that the total conductivity increased with temperature. Although a very small amount of impurity phases exists in the sample, the conductivity must be due to the contribution of the main phase of $PrBaMnMoO_{6-\delta}$ (> 95%). Moreover, from the literature, it has been proven that scheelite structure $BaMoO_4$ shows very low conductivity [56,57]. *In-situ* structure-conductivity measurement simply allows to understand the properties in more realistic or noble conditions. The Argon gas was used to create a chemically-inert atmosphere to prevent oxidation of the electrodes. The phase fractions were extracted from the diffraction data collected from Rietveld refinement. This study proves that $PrBaMnMoO_{6-\delta}$ is structurally stable and highly conductive at elevated temperatures.

4. Conclusions

This research demonstrated a novel approach of *in-situ* structure and conductivity measurement using neutron diffraction. Double perovskite-type $PrBaMnMoO_{6-\delta}$ exhibits a monoclinic crystal structure in the $P2_1/n$ space group and there were no distinct phase changes observed at higher temperatures. SEM analysis of the microstructure showed a significantly porous matrix with distinctive grain borders. The analysis of impedance spectra revealed that the total conductivity of $PrBaMnMoO_{6-\delta}$ considerably increased with temperature. The maximum conductivity of 130.84 Scm^{-1} was achieved at 700 °C. Through these observations, we were able to successfully determine the phase stability, porosity and conductivity of $PrBaMnMoO_{6-\delta}$. These characteristics can contribute to the high potential of the double perovskite being utilized as electrode materials in SOFCs. The authors recommend the use of *in-situ* studies to further enhance the development of electrodes for SOFCs.

Declaration of competing interest

The authors declare that they have no known competing financial interests or personal relationships that could have appeared to influence the work reported in this paper.

Acknowledgement

The authors gratefully acknowledge the UBD Graduate Scholarship (UGS) awarded to Shammya Afroze. The authors are extremely grateful to Professor Sten G. Eriksson, Department of Chemistry and Chemical Engineering, at the Chalmers University of Technology. The authors would also like to show gratitude to the ISIS Neutron and Muon facility in the UK for their scheduled beam-time (RB1810638, DOI: https://doi.org/10.5286/ISIS.E.RB1810638). The authors would further like to thank Dr. Aminul Islam and the SEM laboratory of the Department of Geological Sciences at Universiti Brunei Darussalam for their support in the use of the SEM.

References

[1] Y. Zhang, H. Zhao, Z. Du, K. Świerczek, Y. Li, High-performance SmBaMn2O5+δ electrode for symmetrical solid oxide fuel cell, Chem. Mater. 31 (2019) 3784–3793, https://doi.org/10.1021/acs.chemmater.9b01012.
[2] S. Afroze, N. Torino, P.F. Henry, M. Sumon Reza, Q. Cheok, A.K. Azad, Insight of novel layered perovskite PrSrMn2O5+δ: a neutron powder diffraction study, Mater. Lett. 261 (2020) 127126, https://doi.org/10.1016/j.matlet.2019.127126.
[3] J. Jeong, A.K. Azad, H. Schlegl, B. Kim, S.-W. Baek, K. Kim, H. Kang, J.H. Kim, Structural, thermal and electrical conductivity characteristics of Ln 0.5 Sr 0.5 Ti 0.5 Mn 0.5 O 3\pmd (Ln: La, Nd and Sm) complex perovskites as anode materials for solid oxide fuel cell, J. Solid State Chem. 226 (2015) 154–163.
[4] S. Afroze, M.S. Reza, Q. Cheok, J. Taweekun, A.K. Azad, Solid oxide fuel cell (SOFC); A new approach of energy generation during the pandemic COVID-19, Int. J. Integr. Eng. 12 (2020) 245–256, https://doi.org/10.30880/ijie.2020.12.05.030.
[5] N. Radenahmad, S. Afroze, A. Afif, A.T. Azad, J.S. Shin, J.Y. Park, J.H. Zaini, A.K. Azad, High conductivity and high density SrCe0.5Zr0.35Y0.1A0.05O3-δ (A = Gd, Sm) proton-conducting electrolytes for IT-SOFCs, Ionics 26 (2020) 1297–1305, https://doi.org/10.1007/s11581-019-03278-w.
[6] M.S. Reza, S.N. Islam, S. Afroze, M.S. Abu Bakar, R.S. Sukri, S. Rahman, A.K. Azad, Evaluation of the bioenergy potential of invasive Pennisetum purpureum through pyrolysis and thermogravimetric analysis, Energy, Ecol. Environ. 5 (2020) 118–133, https://doi.org/10.1007/s40974-019-00139-0.
[7] M.S. Reza, C.S. Yun, S. Afroze, N. Radenahmad, M.S.A. Bakar, R. Saidur, J. Taweekun, A.K. Azad, Preparation of activated carbon from biomass and its' applications in water and gas purification, a review, Arab J. Basic Appl. Sci. 27 (2020) 208–238, https://doi.org/10.1080/25765299.2020.1766799.
[8] M.S. Reza, A. Ahmed, W. Caesarendra, M.S. Abu Bakar, S. Shams, R. Saidur, N. Aslfattahi, A.K. Azad, Acacia Holosericea, An invasive species for bio-char, bio-oil, and biogas production, Bioengineering 6 (2019) 33, https://doi.org/10.3390/bioengineering6020033.
[9] M.S. Reza, S. Afroze, M.S.A. Bakar, R. Saidur, N. Aslfattahi, J. Taweekun, A.K. Azad, Biochar characterization of invasive Pennisetum purpureum grass: effect of pyrolysis temperature, Biochar 2 (2020) 239–251, https://doi.org/10.1007/s42773-020-00048-0.
[10] R.J. Payne, J. Love, M. Kah, CFCL's BlueGen product, ECS Trans. (2011) 81–85, https://doi.org/10.1149/1.3569981.
[11] N. Radenahmad, A.T. Azad, M. Saghir, J. Taweekun, M.S.A. Bakar, M.S. Reza, A.K. Azad, A review on biomass derived syngas for SOFC based combined heat and power application, Renew. Sustain. Energy Rev. 119 (2020) 109560, https://doi.org/10.1016/j.rser.2019.109560.
[12] Danbury fair becomes the first bloom energy powered shopping mall | bloom energy (n.d.)(accessed January 13, 2019), https://www.bloomenergy.com/newsroom/press-releases/danbury-fair-becomes-first-bloom-energy-powered-shopping-mall.
[13] W.H. Kan, V. Thangadurai, Challenges and prospects of anodes for solid oxide fuel cells (SOFCs), Ionics 21 (2015) 301–318, https://doi.org/10.1007/s11581-014-1334-6.
[14] A. Ghosh, A. Azad, J.T. Irvine, Study of Ga doped LSCM as an anode for SOFC, ECS Trans. (2011) 1337–1343, https://doi.org/10.1149/1.3570120.
[15] C. Xia, M. Liu, Microstructures, conductivities, and electrochemical properties of Ce0.9Gd0.1O2 and GDC–Ni anodes for low-temperature SOFCs, Solid State Ionics 152–153 (2002) 423–430, https://doi.org/10.1016/S0167-2738(02)00381-8.
[16] D. Neagu, J.T.S. Irvine, Structure and properties of La 0.4 Sr 0.4 TiO 3 ceramics for use as anode materials in solid oxide fuel cells, Chem. Mater. 22 (2010) 5042–5053, https://doi.org/10.1021/cm101508w.
[17] P. Steiger, D. Burnat, H. Madi, A. Mai, L. Holzer, J. Van Herle, O. Kröcher, A. Heel, D. Ferri, Sulfur poisoning recovery on a solid oxide fuel cell anode material through reversible segregation of nickel, Chem. Mater. 31 (2019) 748–758, https://doi.org/10.1021/acs.chemmater.8b03669.
[18] D. Marrero-López, J. Peña-Martínez, J.C. Ruiz-Morales, D. Pérez-Coll, M.A.G. Aranda, P. Núñez, Synthesis, phase stability and electrical conductivity of Sr2MgMoO6-δ anode, Mater. Res. Bull. 43 (2008) 2441–2450, https://doi.org/10.1016/j.materresbull.2007.07.032.
[19] Z. Wang, Y. Tian, Y. Li, Direct {CH4} fuel cell using Sr2FeMoO6 as an anode material, J. Power Sources 196 (2011) 6104–6109, https://doi.org/10.1016/j.jpowsour.2011.03.053.
[20] A.K. Azad, J.H. Kim, J.T.S. Irvine, Structure–property relationship in layered perovskite cathode LnBa0.5Sr0.5Co2O5+δ (Ln=Pr, Nd) for solid oxide fuel cells, J. Power Sources 196 (2011) 7333–7337, https://doi.org/10.1016/j.jpowsour.2011.02.063.
[21] W. He, X. Wu, F. Dong, M. Ni, A novel layered perovskite electrode for symmetrical

solid oxide fuel cells: PrBa(Fe0.8Sc0.2)2O5+δ, J. Power Sources 363 (2017) 16–19, https://doi.org/10.1016/j.jpowsour.2017.07.059.
[22] A.K. Azad, J.T.S. Irvine, Characterization of YSr2Fe3O8−δ as electrode materials for SOFC, Solid State Ionics 192 (2011) 225–228, https://doi.org/10.1016/j.ssi.2010.11.027.
[23] M.C. Knapp, P.M. Woodward, A-site cation ordering in AA′BB′O6 perovskites, J. Solid State Chem. 179 (2006) 1076–1085, https://doi.org/10.1016/J.JSSC.2006.01.005.
[24] A.K. Azad, Synthesis, Structure, and Magnetic Properties of Double Perovskites of the Type A2MnBO6 and A2FeBO6;(A= Ca, Sr, Ba, La; B= W, Mo, Cr, Chalmers Reproservice AB, 2004.
[25] M.T. Anderson, K.B. Greenwood, G.A. Taylor, K.R. Poeppelmeier, B-cation arrangements in double perovskites, Prog. Solid State Chem. 22 (1993) 197–233, https://doi.org/10.1016/0079-6786(93)90004-B.
[26] J. Zou, J. Park, B. Kwak, H. Yoon, J. Chung, Effect of Fe doping on PrBaCo 2O 5 + δ as cathode for intermediate-temperature solid oxide fuel cells, Solid State Ionics 206 (2012) 112–119, https://doi.org/10.1016/j.ssi.2011.10.025.
[27] A.C. Tomkiewicz, M.A. Tamimi, S. Mcintosh, Structural Analysis of PrBaMn2O5+δ under SOFC Anode Conditions by In-Situ Neutron Powder Diffraction vol. 330, (2016), pp. 240–245, https://doi.org/10.1016/j.jpowsour.2016.09.013.
[28] D. Chen, R. Ran, K. Zhang, J. Wang, Z. Shao, Intermediate-temperature electrochemical performance of a polycrystalline PrBaCo2O5+δ cathode on samarium-doped ceria electrolyte, J. Power Sources 188 (2009) 96–105, https://doi.org/10.1016/j.jpowsour.2008.11.045.
[29] K. Zhang, L. Ge, R. Ran, Z. Shao, S. Liu, Synthesis, characterization and evaluation of cation-ordered LnBaCo 2 O 5+d as materials of oxygen permeation membranes and cathodes of SOFCs, Acta Mater. 56 (2008) 4876–4889, https://doi.org/10.1016/j.actamat.2008.06.004.
[30] S. Sengodan, S. Choi, A. Jun, T.H. Shin, Y.-W. Ju, H.Y. Jeong, J. Shin, J.T.S. Irvine, G. Kim, Layered oxygen-deficient double perovskite as an efficient and stable anode for direct hydrocarbon solid oxide fuel cells, Nat. Mater. 14 (2015) 205–209, https://doi.org/10.1038/nmat4166.
[31] M.T. Anderson, J.T. Vaughey, K.R. Poeppelmeier, Structural similarities among oxygen-deficient perovskites, Chem. Mater. 5 (1993) 151–165, https://doi.org/10.1021/cm00026a003.
[32] A.K. Azad, A. Kruth, J.T.S. Irvine, Influence of atmosphere on redox structure of BaCe0.9Y 0.1O2.95 - insight from neutron diffraction study, Int. J. Hydrogen Energy 39 (2014) 12804–12811, https://doi.org/10.1016/j.ijhydene.2014.05.080.
[33] S. Tao, J.T.S. Irvine, Observed by in situ high-temperature neutron powder diffraction, Chem. Mater. 18 (2006) 5453–5460, https://doi.org/10.1021/cm061413n.
[34] T.E. Engin, A.V. Powell, R. Haynes, M.A.H. Chowdhury, C.M. Goodway, R. Done, O. Kirichek, S. Hull, A high temperature cell for simultaneous electrical resistance and neutron diffraction measurements, Rev. Sci. Instrum. 79 (2008) 095104, , https://doi.org/10.1063/1.2979011.
[35] A.K. Azad, S.A. Ivanov, S.G. Eriksson, J. Eriksen, H. Rundlöf, R. Mathieu, P. Svedlindh, Nuclear and magnetic structure of Ca2MnWO6: a neutron powder diffraction study, Mater. Res. Bull. 36 (2001) 2485–2496, https://doi.org/10.1016/S0025-5408(01)00708-5.
[36] A.K. Azad, S.G. Eriksson, S.A. Ivanov, H. Rundlöf, J. Eriksen, R. Mathieu, P. Svedlindh, Structural and magnetic characterisation of the double perovskites AA'MnWO6 (AA' = Ba2, SrBa, Sr2, SrCa and Ca2), Ferroelectrics 269 (2002) 105–110, https://doi.org/10.1080/00150190211167.
[37] S. Afroze, A.M. Abdalla, N. Radenahmad, Q.C. Hoon Nam, A.K. Azad, Synthesis, structural and thermal properties of double perovskite NdSrMn2O6 as potential anode materials for solid oxide fuel cells, IET Conf. Publ. (2018) 1–4, https://doi.org/10.1049/cp.2018.1588.
[38] S. Afroze, N. Torino, P.F. Henry, M.S. Reza, Q. Cheok, A.K. Azad, Neutron and X-ray powder diffraction data to determine the structural properties of novel layered perovskite PrSrMn2O5+δ, Data Br 29 (2020) 105173, https://doi.org/10.1016/j.dib.2020.105173.
[39] FullProf suite homepage (n.d.) accessed, https://www.ill.eu/sites/fullprof/ , Accessed date: 4 December 2019.
[40] R.I. Smith, S. Hull, M.G. Tucker, H.Y. Playford, D.J. McPhail, S.P. Waller, S.T. Norberg, The upgraded Polaris powder diffractometer at the ISIS neutron source, Rev. Sci. Instrum. 90 (2019) 115101–115113, https://doi.org/10.1063/1.5099568.
[41] S. Hull, R.I. Smith, W.I.F. David, A.C. Hannon, J. Mayers, R. Cywinski, The Polaris powder diffractometer at ISIS, Phys. B Phys. Condens. Matter. 180-181 (1992) 1000–1002, https://doi.org/10.1016/0921-4526(92)90533-X.
[42] F.G. Kinyanjui, S.T. Norberg, I. Ahmed, S.G. Eriksson, S. Hull, In-situ conductivity and hydration studies of proton conductors using neutron powder diffraction, Solid State Ionics 225 (2012) 312–316, https://doi.org/10.1016/J.SSI.2012.05.018.
[43] B.H. Toby, R.B. Von Dreele, GSAS-II : the genesis of a modern open-source all purpose crystallography software package, J. Appl. Crystallogr. 46 (2013) 544–549, https://doi.org/10.1107/S0021889813003531.
[44] A guide to scanning microscope observation JEOL serving advanced technology, n.d. accessed https://www.jeol.co.jp/en/applications/pdf/sm/844_en.pdf , Accessed date: 4 April 2019.
[45] A. Muñoz, J.A. Alonso, M.T. Casais, M.J. Martínez-Lope, M.T. Fernández-Díaz, Crystal and magnetic structure of the complex oxides Sr2MnMoO6, Sr2MnWO6 and Ca2MnWO6: a neutron diffraction study, J. Phys. Condens. Matter 14 (2002) 8817–8830, https://doi.org/10.1088/0953-8984/14/38/306.
[46] Q. Zhang, T. Wei, Y.-H. Huang, Electrochemical performance of double-perovskite Ba2MMoO6 (M=Fe, Co, Mn, Ni) anode materials for solid oxide fuel cells, J. Power Sources 198 (2012) 59–65, https://doi.org/10.1016/j.jpowsour.2011.09.092.
[47] Jinmin Zhang, Danian Ye, C.T. Prewitt, Relationship between the unit-cell volumes and cation radii of isostructural compounds and the additivity of the molecular volumes of carbonates, Am. Mineral. 76 (1991) 100–105.
[48] Y. Zhang, Z. Su, A.K. Azad, W. Zhou, J.T.S. Irvine, Directly imaging interstitial oxygen in silicate apatite, Adv. Energy Mater. 2 (2012) 316–321.
[49] J.A. Gómez-Cuaspud, E. Vera-López, Synthesis and characterization of La0.8Sr0.2Ni(1−x)CrxO3 (x = 0.0, 0.2, 0.4, 0.6, 0.8, 1.0) system by the combustion method, Boletín La Soc, Española Cerámica y Vidr 56 (2017) 273–282, https://doi.org/10.1016/J.BSECV.2017.05.004.
[50] M. Gerstl, E. Navickas, G. Friedbacher, F. Kubel, M. Ahrens, J. Fleig, The separation of grain and grain boundary impedance in thin yttria stabilized zirconia (YSZ) layers, Solid State Ionics 185 (2011) 32–41, https://doi.org/10.1016/j.ssi.2011.01.008.
[51] S.M.H. Rahman, S.T. Norberg, C.S. Knee, J.J. Biendicho, S. Hull, S.G. Eriksson, Proton conductivity of hexagonal and cubic BaTi 1−x Sc x O 3−δ (0.1 ≤ x ≤ 0.8), Dalton Trans. 43 (2014) 15055–15064, https://doi.org/10.1039/C4DT01280A.
[52] R. Singh, G.S. Sandhu, R. Penna, I. Farina, Investigations for thermal and electrical conductivity of ABS-graphene blended prototypes, Materials 10 (2017) 881, https://doi.org/10.3390/ma10080881.
[53] S.M.H. Rahman, S.T. Norberg, C.S. Knee, J.J. Biendicho, S. Hull, S.G. Eriksson, Proton conductivity of hexagonal and cubic BaTi1−xScxO3−Δ (0.1 ≤ x ≤ 0.8), J. Chem. Soc., Dalton Trans. 43 (2014) 15055–15064, https://doi.org/10.1039/c4dt01280a.
[54] S. Ji, H.G. Seo, S. Lee, J. Seo, Y. Lee, W.H. Tanveer, S.W. Cha, W. Jung, Integrated design of a Ni thin-film electrode on a porous alumina template for affordable and high-performance low-temperature solid oxide fuel cells, RSC Adv. 7 (2017) 23600–23606, https://doi.org/10.1039/c7ra02719b.
[55] J.-D. Kim, G.-D. Kim, J.-W. Moon, Y.-I. Park, W.-H. Lee, K. Kobayashi, M. Nagai, C.-E. Kim, Characterization of LSM-YSZ composite electrode by ac impedance spectroscopy, Solid State Ionics 143 (2001) 379–389, https://doi.org/10.1016/S0167-2738(01)00877-3.
[56] N. Nallamuthu, I. Prakash, M. Venkateswarlu, N. Satyanarayana, Preparation, characterisation and electrical conductivity studies of nanocrystalline BaMoO4 material, Nanotechnol. 2009 Fabr. Part. Charact. MEMS, Electron. Photonics, - Tech. Proc. 2009 NSTI Nanotechnol. Conf. Expo, NSTI-Nanotech 1 (2009) 155–158 2009.
[57] A. Afif, J. Zaini, S.M.H. Rahman, S. Eriksson, M.A. Islam, A.K. Azad, Scheelite type Sr1−xBaxWO4 (x = 0.1, 0.2, 0.3) for possible application in Solid Oxide Fuel Cell electrolytes, Sci. Rep. 9 (2019), https://doi.org/10.1038/s41598-019-45668-0.